New ocean subsurface optical properties from space lidars: CALIOP/CALIPSO and ATLAS/ICESat-2

X. Lu[1,2], Y. Hu[2], Y. Yang[3], T. Neumann[3], A. Omar[2], R. Baize[2], M. Vaughan[2], S. Rodier[1,2], B. Getzewich[2], Pat Lucker[1,2], Chip Trepte[2], C. Hostetler[2], and D. Winker[2]

[1]Science Systems and Applications, Inc., Hampton, VA, 23666, USA.

[2]NASA Langley Research Center, Hampton, VA, 23681, USA.

[3]NASA Goddard Space Flight Center, Greenbelt, MD, 20771, USA.

Corresponding author: Xiaomei Lu (xiaomei.lu@nasa.gov); Yongxiang Hu (yongxiang.hu-1@nasa.gov)

Key Points:

- Global ocean subsurface properties are retrieved from CALIOP.
- The CALIOP crosstalk artifact and ATLAS after pulsing effects are removed.
- High vertical resolution of ocean subsurface profiles can be obtained from ATLAS/ICESat-2.
- The ocean subsurface high vertical resolution profiles are observed from space for the first time by ICESat-2.

Abstract

Remote sensing from Earth-observing satellites is now providing valuable information about the ocean phytoplankton distributions. This paper presents the new ocean subsurface optical properties obtained from two space-based lidars: the Cloud-Aerosol Lidar with Orthogonal Polarization (CALIOP) aboard Cloud-Aerosol Lidar and Infrared Pathfinder Satellite Observations (CALIPSO) satellite and the Advanced Topographic Laser Altimeter System (ATLAS) aboard Ice, Cloud, and land Elevation Satellite-2 (ICESat-2) satellite. Obtaining reliable estimates of subsurface biomass necessitates removing instrument artifacts peculiar to each sensor; i.e., polarization crosstalk artifacts in the CALIOP signals and after pulsing effects arising from the ATLAS photodetectors. We then validate the lidar retrieved optical properties with MODerate-resolution Imaging Spectroradiometer (MODIS) ocean color measurements and autonomous biogeochemical Argo float profiles. Our results support the continued use of present and future spaceborne lidars to study the global plankton system and characterize its vertical structures in the upper ocean.

1 Introduction

Ocean color remote sensing entered a new era with the launch of the National Aeronautics and Space Administration (NASA) Coastal Zone Color Scanner (CZCS) in 1978 (Sullivan et al., 1993). For the first time, maps of phytoplankton biomass (chlorophyll) - a key measurement of marine ecosystems - could be produced from space observations, with the potential for daily to interannual observations at ocean basin scales. Regional to global maps of phytoplankton chlorophyll and other products derived from satellite measurements of water-leaving radiance are now accessible to users all over the world and have become an essential tool for the study and analysis of ocean biogeochemistry and ocean ecosystems. For decades, ocean color remote sensing has led to unprecedented scientific understanding in global ocean biology and biogeochemistry. However, because previous ocean color measurements have relied solely on passive remote sensing techniques, the data coverage is limited to the uppermost portion of the water column and is unable to resolve underlying vertical structure (Hostetler et al., 2018; Jamet et al., 2019). Moreover, passive sensors (e.g. MODerate-resolution Imaging Spectroradiometer, MODIS) only provide ocean color records during daytime. As a result, vast ocean areas in high latitudes during polar night remain unsampled and places for which data are available typically provide information for only a few months in each calendar year.

Estimates of global phytoplankton distributions from a space-based lidar was first demonstrated (Behrenfeld et al., 2013) using measurements from the Cloud-Aerosol Lidar with Orthogonal Polarization (CALIOP). CALIOP is a dual-wavelength (532 nm and 1064 nm), polarization sensitive (at 532 nm) elastic backscatter lidar that has been making measurements from the Cloud-Aerosol Lidar and Infrared Pathfinder Satellite Observations (CALIPSO) satellite since June 2006 (Hunt et al., 2009; David M. Winker et al., 2009). Using the CALIOP depolarization ratio measurements at 532 nm, together with co-located A-Train measurements, such as Advanced Microwave Scanning Radiometer - Earth observing system (AMSR-E) wind speeds and MODIS diffuse attenuation coefficients, innovative retrieval methods have been developed to translate the CALIOP ocean backscattered signals into ocean optical properties, such as the particulate backscatter coefficient, (b_{bp}, m^{-1}) (Behrenfeld et al., 2013; Lacour et al., 2020; Lu et al., 2016), phytoplankton biomass (Behrenfeld et al., 2017) and total depolarization ratio of ocean waters (Dionisi et al., 2020; Lu et al., 2014). However, CALIOP's coarse vertical resolution

(30 m in the atmosphere, 22.5 m in the water) (Behrenfeld et al., 2013; Lu et al., 2014) and the non-ideal transient response of the 532 nm detectors (Hu et al., 2007; Lu et al., 2018; Lu et al., 2020) present substantial challenges in retrieving ocean subsurface profiles directly from CALIOP measurements.

On 15 September 2018, the Ice, Cloud, and land Elevation Satellite-2 (ICESat-2) mission launched from Vandenberg Air Force Base, CA carrying the Advanced Topographic Laser Altimeter System (ATLAS) (Markus et al., 2017). ATLAS is a 532 nm photon-counting laser altimeter with a 10 kHz pulse repetition rate and a footprint diameter of 11 m at the Earth's surface (Magruder et al., 2020; Magruder & Brunt, 2018; Markus et al., 2017). The ATLAS instrument architecture differs significantly from CALIOP, allowing it to overcome many of CALIOP's subsurface deficiencies. Our collaborative team onsite at NASA's Langley Research Center (LaRC) and Goddard Space Flight Center (GSFC) has derived a set of new ocean data products from ATLAS/ICESat-2 measurements (Lu et al., 2019; Lu, Hu, Yang, et al., 2020), which, for the first time, quantify the vertical distribution of phytoplankton optical properties below the ocean surface from space. The vertical structure of these subsurface optical properties is not available in the existing ocean color record generated from passive remote sensing measurements (Hovis et al., 1980), hence the ATLAS/ICESat-2 ocean results can provide unique new information that augments existing ocean color measurements by adding the depth dimension with high horizontal and vertical resolution measurements during both day and night.

Here we focus on retrieving ocean subsurface optical properties using both CALIOP and ATLAS measurements. For both systems, measurement artifacts such as CALIOP's polarization crosstalk (Supplementary Text S1) and the ATLAS's after pulsing effects (Supplementary Text S2) are removed in order to obtain reliable ocean subsurface results. The cross-polarization component of the ocean subsurface backscatter ($\gamma_{\perp}$, sr^{-1}) and subsurface depolarization ratio (δ_{sub}) are retrieved globally from the CALIOP version 4.1 level 1b data product (Getzewich et al., 2018; Kar et al., 2018). We use ATLAS geolocated photon data of ATL03 Release 003 (Neumann et al., 2020) to quantify the vertical distribution of ocean subsurface properties (Lu et al., 2019; Lu, Hu, Yang, et al., 2020), such as the profiles of subsurface attenuated backscatter coefficient (β, $m^{-1}sr^{-1}$), total and particulate basckscattering coefficients (b_b and b_{bp}, m^{-1}). These lidar derived properties are then validated using autonomous biogeochemical Argo float profiles (Argo, 2020; Claustre et al., 2010; Organelli et al., 2017) and MODIS ocean color records (NASA, 2018).

2 CALIOP new global ocean subsurface results

2.1 CALIOP data and methods

The CALIOP lidar was designed to provide the observations necessary for an improved understanding of the impact of clouds and aerosols on the Earth's radiation budget and climate (Winker et al., 2010). Since launch, newly developed applications of CALIOP data for plankton retrievals (Behrenfeld et al., 2013, 2016, 2019; Lu et al., 2014) on the global scale, including high latitude regions during polar night, have provided a first glimpse into a 'new lidar era in satellite oceanography' (Dionisi et al., 2020; Hostetler et al., 2018; Jamet et al., 2019).

However, non-ideal polarization separation by the optical components in CALIOP receiver can cause some small fraction of the backscattered optical power polarized parallel to the receiver reference plane to be misdirected into the perpendicular channel, and vice versa (Hostetler et al., 2006). This effect, known as polarization crosstalk, typically causes the measured cross-polarized

(i.e., perpendicular channel) attenuated backscatter coefficient ($\beta'_{\perp}$, $m^{-1}sr^{-1}$) to be higher than its true value and the measured co-polarized (i.e., parallel channel) attenuated backscatter coefficient ($\beta'_{\parallel}$, $m^{-1}sr^{-1}$) lower than its true value. For ocean backscattered signals, the relative errors in the CALIOP measured cross-polarized attenuated backscatter coefficient ($\frac{\beta'_{\perp,measured}-\beta'_{\perp,correct}}{\beta'_{\perp,correct}} \times 100\%$) due to crosstalk can be up to 100% or more (Supplementary Text S1), which in turn will introduce biases into the subsequently derived ocean optical properties, such as particulate backscattering coefficient b_{bp}, phytoplankton biomass, total particulate organic carbon (*POC*) stocks, and etc. Consequently, estimates of ocean optical properties from CALIOP measurements must take crosstalk into account. However, previous analyses of CALIOP level 1 data for ocean properties retrievals (Behrenfeld et al., 2013; Bisson et al., 2021; Dionisi et al., 2020; Lacour et al., 2020; Lu et al., 2014) did not take into account the effect of optical crosstalk between the 532 nm co-polarized and cross-polarized channels.

The new CALIOP ocean subsurface results reported in this paper are corrected for the crosstalk effect. Details on estimating the crosstalk values are provided in supplementary Text S1. Figure S1 shows the time series of crosstalk values over the CALIOP mission (June 2006 to November 2020). Briefly, if the magnitude of the crosstalk is known, crosstalk-corrected signals can be derived from the measured signals in a straightforward manner (Pitts et al., 2018) (suplementatry Text S1.2). Using CALIOP crosstalk-corrected signals is highly recommended for all ocean subsurface studies.

2.2 Global CALIOP $\gamma_{\perp}$ and δ_{sub}

The new global cross-polarization component of the total ocean subsurface backscatter ($\gamma_{\perp}$, sr^{-1}) is obtained from CALIOP crosstalk-corrected ocean attenuated backscatter coefficients ($\beta'_{\parallel,\mathrm{correct}}$, $\beta'_{\perp,\mathrm{correct}}$) as indicated in Eq. (6) of supplementary text S1.2. The AMSR-E (2006-2011) and Modern-Era Retrospective Analysis for Research and Applications-version 2 (MERRA-2) (2011-2020) wind speeds were used to calibrate the atmospheric two-way transmission (Hu et al., 2008; Lu et al., 2014) (Supplementary Text S1). The CALIOP data are seasonally averaged for the 2008-2020 period and binnned to 1º latitude by 1º lontgitude pixels (Figs. 1-3). Unlike the co-polarization signal ($\gamma_{||}$, sr^{-1}), which can be contaminated by ocean surface reflection, the $\gamma_{\perp}$ is due almost entirely to backscatter from ocean subsurface particulate matter (Behrenfeld et al., 2013; Lu et al., 2016). The global distributions of $\gamma_{\perp}$ during both nighttime (Figure 1) and daytime (Figure 2) exhibit all the major ocean plankton fearures anticipated from the earlier data record, such as Fig. S2 of global ocean remote sensing reflectance at 531 nm from MODIS measurements. The low values of $\gamma_{\perp}$ over most of the permanently stratified ocean (roughly between 40ºN and 40ºS latitudes) are stable over the annual cycle, indicating low nutrient, low biomass waters, except in coastal regions and the Eastern Pacific upwelling region. The seasonal changes of $\gamma_{\perp}$ (Figures 1a to 1d, and Figures 2a to 2d) illustrate the strong seasonality of high latitude phytoplankton communities. For example, the elevated $\gamma_{\perp}$ values in the subarctic oceans reflect the large summer (June - August) phytoplankton bloom (Figures 1b and 2b), while $\gamma_{\perp}$ in the Southern Oceans reflect the large winter (December - February) bloom (Figures 1d and 2d). The high latitude $\gamma_{\perp}$ (Figure 1 vs. 2) also indicate the day-night differences, which is useful for further studies of day-night differences in phytoplankton removal rates.

The new CALIOP-detrived $\gamma_{\perp}$ is a fundamental parameter that can be used as the input to retrieve high level ocean subsurface properties such as δ_{sub}, b_{bp} and *POC* (Behrenfeld et al., 2013;

Lu et al., 2014). The lidar-derived depth-integrated attenuated backscatter is comparable to ocean color remote sensing reflectance (Lu, Hu, Yang, et al., 2020). The ocean subsurface depolarization ratio (Figure 3) can be derived by combining CALIOP $\gamma_\perp$ data at 532 nm and MODIS remote sensing reflectance (*Rrs*, sr^{-1}) data at 531 nm (Fig. S2) as follows: $\delta_{sub} = \frac{\gamma_\perp}{Rrs-\gamma_\perp}$. The *Rrs*-$\gamma_\perp$ represents the co-polarization component of the total subsurface backscatter. For comparisons, global seasonal maps of CALIOP-derived total depolarization ratio ($\delta_{total} = \frac{\gamma_\perp}{\gamma_\parallel}$), including both surface and subsurface contributions, are provided in Figures S3 and S4. Due to ocean surfaces contributions, δ_{total} is less than 0.1 for most of the global ocean. There are very few published measurements of below surface depolarization ratios, with global spatial and seasonal distributions being especially rare. The newly derived δ_{sub} shown in Figure 3 provides some initial insights into the below surface particulate matter shape, which should be particularly useful for studies of phytoplankton communities and diversity in the global ocean (Righetti et al., 2019; Vallina et al., 2014). Uncertainties in the derivation of δ_{sub} depend on the calibraion of both CALIOP $\gamma_\perp$ and MODIS *Rrs*. Assuming a 10% uncertainty for MODIS *Rrs* (Hu et al., 2013) and CALIOP $\gamma_\perp$, the uncertainty of δ_{sub} is ~14%. We are currently conducting a study to estimate the co-polarization component of the total subsurface backscatter from CALIOP co-polarization channel, where the ocean surface contribution to co-polarization signal magnitude will be estimated from 1064 nm channel. Upon successful conclusion of this effort, we will also be able to provide the ocean subsurface depolarization ratio during nighttime.

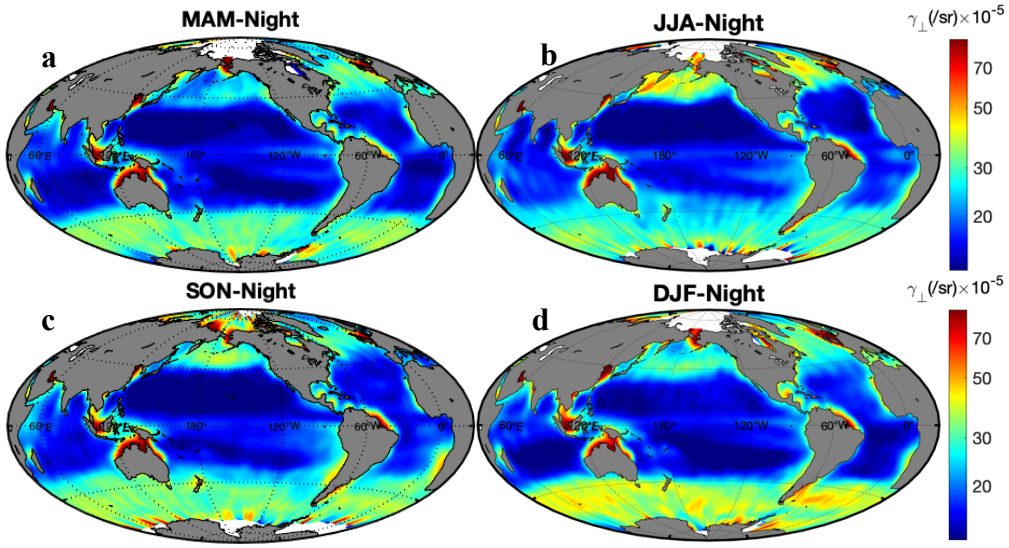

Figure 1. Seasonal changes of CALIOP cross-polarization component of the ocean subsurface backscatter ($\gamma_\perp$, sr^{-1}) during nighttime: (a) March - May; (b) June - August; (c) September -

November; (d) December - February. Data are seasonally averaged climatologies for the 2008-2020 period binned to 1º latitude × 1º longitude pixels.

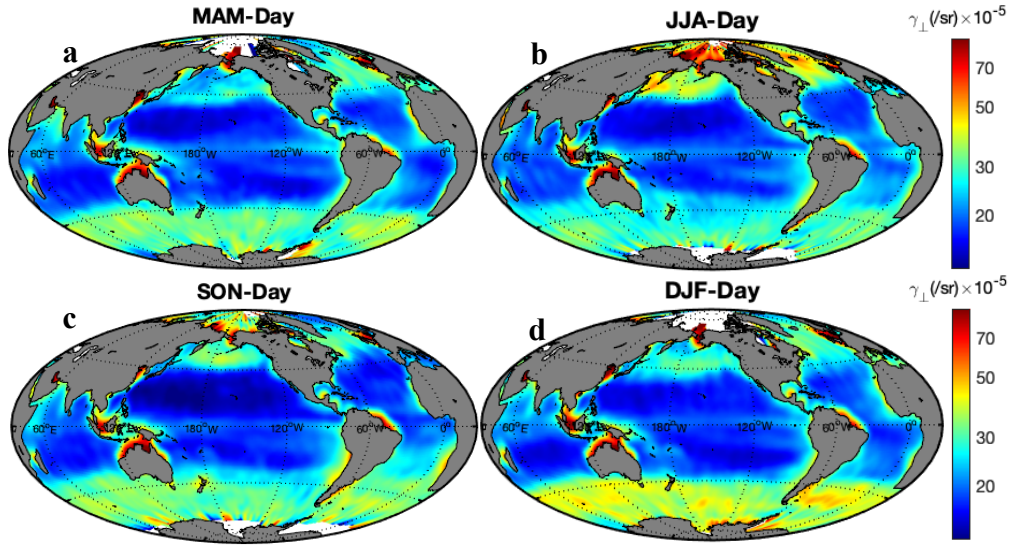

Figure 2. Same as Figure 1 but for daytime results.

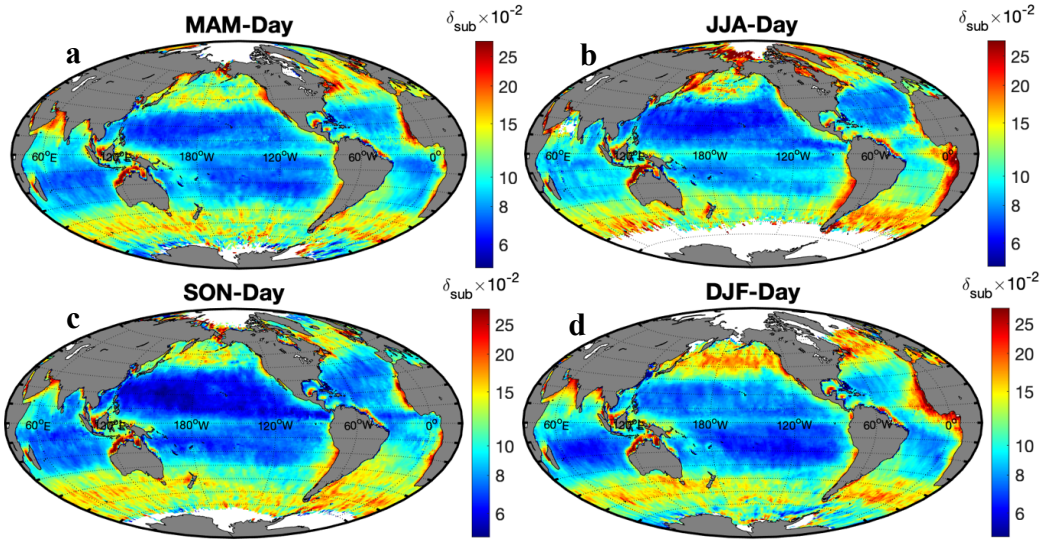

Figure 3. Seasonal changes of subsurface depolarization ratio (δ_{sub}) during daytime: (a) March - May; (b) June - August; (c) September - November; (d) December - February. Data are seasonally averaged climatologies for the 2008-2020 period binned to 1º latitude × 1º longitude pixels.

3 ATLAS ocean subsurface high vertical resolution profiles

3.1 ATLAS data and methods

ICESat-2 is a follow-on to the original ICESat mission (Abshire et al., 2005) that provides global altimetry and atmospheric measurements with particular emphasis on surface elevation changes in the polar regions (Markus et al., 2017). ATLAS uses photomultiplier tubes (PMTs) as detectors in photon counting mode, so that a single photon reflected back to the receiver triggers a detection within the ICESat-2 data acquisition system. The single-photon-sensitive detection

technique used by ATLAS to measure photon time of flight provides the very high vertical resolution required to detect small spatial and temporal changes in polar ice elevations (Neumann et al., 2019; Popescu et al., 2018). Many other areas of Earth science also benefit from the ICESat-2 mission. For the atmospheric community, ICESat-2 delivers calibrated attenuated backscatter profiles, cloud and aerosol heights, and column optical depths (Palm et al., 2020). The hydrological community uses ICESat-2 measurements to determine global inland water body heights and associated properties (Jasinski et al., 2016). Similarly, the oceanography community can readily obtain shallow water bathymetry and global ocean and wave heights (Morison et al. 2019).

In addition, the ICESat-2 detected photon events over ocean regions provide great opportunity for ocean subsurface studies (Lu et al., 2019; Lu, Hu, Yang, et al., 2020). Details on ocean subsurface properties retrieval methods, including a dedicated deconvolution method to remove ICESat-2 after pulsing effects (e.g., Fig. S5) are given in (Lu, Hu, Yang, et al., 2020) and supplementary text S2. Figure S6 gives the concept and schematic flow chart of applying ICESat-2 ATL03 data for ocean subsurface optical properties retrieval. Briefly, the theoretical ocean surface backscatter at 532 nm is estimated from wind speed (Hu et al., 2008). Then, the calibration coefficients for lidar profiles are the ratios between the theoretical ocean surface backscatter and ATLAS measured photon counts from sea surface. Finally, the profiles of ocean subsurface attanuted backscatter coefficients (e.g., Fig. 4a) are the ATLAS measured subsurface photon counts calibrated by the calibration coefficients. The water optical properties of diffuse attenuation coefficient kd (m^{-1}) and total backscattering coefficient b_b (m^{-1}) are retrieved from the profiles of subsurface attenuated backscatter coefficients (Lu, Hu, Yang, et al., 2020).

The new ocean subsurface results (e.g., Figure 4) from ICESat-2 mission reveal high vertical resolution of subsurface ocean optical properties through the water column that are not available from passive ocean color records or from CALIOP active measurements. The ICESat-2 data thus provide a wealth of unique information to complement existing satellite-based ocean color remote sensing capabilities by adding high spatial and vertical resolution profile measurements during both day and night.

3.2 Evaluation of ATLAS/ICESat-2 ocean results

In situ measurements by autonomous profiling Argo floats (Argo, 2020; Claustre et al., 2010; Organelli et al., 2017) and MODIS-Aqua monthly ocean color products (NASA, 2018) are used to evaluate the ICESat-2 derived ocean results. Details about the Argo float b_{bp} data, MODIS ocean color products, and ICESat-2 ATL03 data used in this paper are provided in the supplementary material.

The two-dimensional distributions of (a) attenuated backscatter coefficient ($\beta(z)$, $m^{-1}sr^{-1}$) and (b) total backscattering coefficient ($b_b(z)$) obtained from ICESat-2 measurement on March 5th 2019 are given in Figure 4. The corresponding ICESat-2 ground tracks and Argo float location (9.32ºS, 141ºW) on March 5th 2019 are shown in Fig. S7 of the supporting document. The horizontal distance between Argo float and ICESat-2 ground track (black line in Fig. 4) is ~ 4.4 km. The seawater backscattering coefficient profile (b_{bw}, m^{-1}) at 532 nm (green dashed line of Fig. 5) is obtained based on the Argo float's temperature and salinity profiles (Werdell et al., 2013). The ICESat-2 vertical profile of subsurface particulate backscattering coefficients, $b_{bp}(z)$ (blue in Fig. 5), corresponding to the vertical black line in Figure 4 is obtained by subtracting the seawater backscattering coefficient (green dashed line in Fig. 5) from total backscattering coefficient (black line in Fig. 4b). Figure 5 shows the vertical profiles of $b_{bp}(z)$ from both the Argo floats and the

ICESat-2 measurements on March 5th 2019. The relative differences between the two b_{bp} profiles, ($\frac{b_{bp,ICESat2}-b_{bp,Argo}}{b_{bp,Argo}} \times 100\%$), are less than 10%, within the known uncertainty of float-derived b_{bp} of ~ 10%-15% (Bisson et al., 2019).

In order to compare with co-located MODIS ocean color results (i.e., layer integrated results), the retrieved ICESat-2 profiles of Fig. 4 are depth-averaged following the method in (Lu, Hu, Yang, et al., 2020) to get layer integrated ocean subsurface attenuated backscatter (Rrs, sr^{-1}) and b_b. The diffuse attenuation coefficient, *kd* (m^{-1}), is derived from the exponential decay of the attenuated backscatter profiles, as one profile shown in Fig. 1 in Lu, Hu, Yang, et al., 2020. Figure 6 shows the comparison between ICESat-2 derived ocean results on March 5th 2019 and co-located MODIS monthly ocean color results in March 2019. Because there are not many MODIS daily measurements co-located with ATLAS/ICESat-2 measurements, the monthly ocean color results co-located with ICESat-2 ground track are used in this work. The mean relative differences of *kd* (m^{-1}), b_b and *Rrs* between ICESat-2 and MODIS measurement are ~7% (Fig. 6a), ~38% (Fig. 6b) and ~18% (Fig. 6c), respectively. These differences are mainly due to the time offset and the different measurement locations (up to 10 km) between ICESat-2 (daily) and MODIS (monthly). The results over the Indian Ocean (Fig. S8-S10 and Table S1) from October 2018 to July 2020 indicate the mean relative differences between ICESat-2 and MODIS are ~11%, ~10% and ~27% for *kd*, b_b and *Rrs*, respectively.

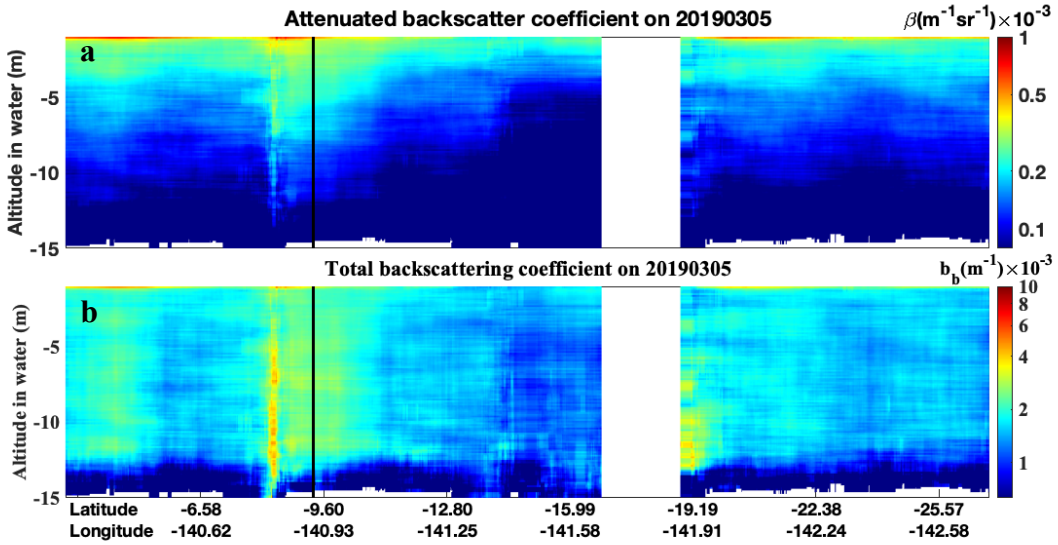

Figure 4. Two-dimensional distributions of (a) attenuated backscatter coefficient (β, $m^{-1}sr^{-1}$) and (b) total backscattering coefficient below ocean surface (b_b, m^{-1}) on March 5th 2019. The x-axis specifies locations along ICESat-2 ground tracks (blue line in Fig. S5) and y-axis is ocean penetration depth in meters. The color bars on the right-hand side provide the range of β and b_b values.

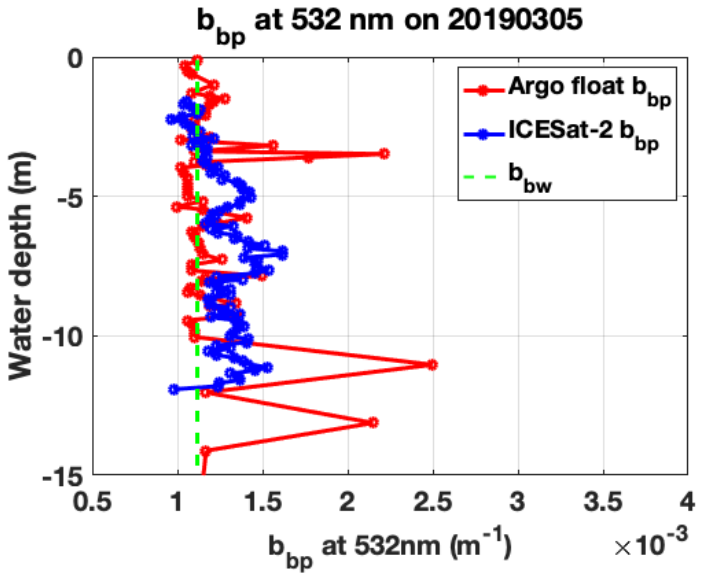

Figure 5. Vertical profiles of particulate backscattering coefficient below ocean surface (b_{bp}, m^{-1}) on March 5th 2019 from ICESat-2 (blue) and Argo float (red). The ICESat-2 profile is located at the black line in Fig. 4. The distance between black line and Argo float is ~ 4.4 km (supplementary Fig. S5). The green dashed line is the seawater backscattering coefficient profile (b_{bw}, m^{-1}) at 532 nm calculated based on Argo float's temperature and salinity vertical profiles on March 5th 2019 at (9.32ºS, 141ºW).

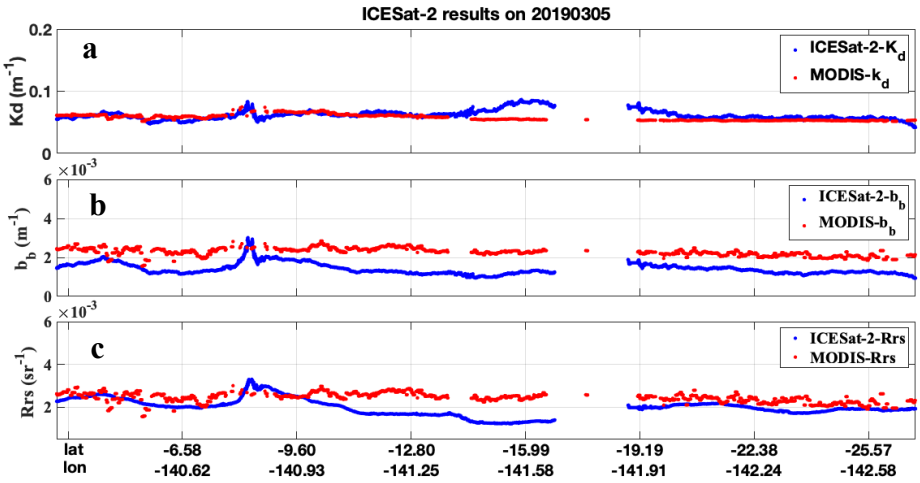

Figure 6. Comparison between ICESat-2 ocean subsurface results (blue) and co-located MODIS monthly mean (red) in March 2019. The ICESat-2 results are from nighttime measurements on March 5th 2019. (a) diffuse attenuation coefficient (m^{-1}); (b) layer-integrated total backscattering coefficient (m^{-1}); (c) layer-integrated ocean subsurface attenuated backscatter (sr^{-1}).

4 Conclusions

New ocean subsurface optical properties are obtained from two space-based lidars: CALIOP/CALIPSO and ATLAS/ICESat-2. For both lidars, measurement artifacts are removed before retrieving ocean optical properties. The global scale CALIOP retrievals and high vertical resolution ATLAS profiles each provide new and unique information that augment the existing

ocean color records acquired by passive remote sensors. This pioneering use of space-based lidars to retrieve ocean subsurface properties will provide a meaningful satellite lidar record to the ocean sciences community, and can help the community to assess the complex interactions involving ocean biology, the cryosphere, and the atmosphere. Moreover, the satellite lidar record will provide important preparatory data for the upcoming Plankton, Aerosol, Cloud, ocean Ecocystem (PACE) mission.

Acknowledgments

The authors would like to thank the NASA CALIPSO, ICESat-2, and MODIS teams for providing the data used in this study. The CALIPSO V4.10 lidar level 1 data used in this study can be freely accessed via https://doi.org/10.5067/CALIOP/CALIPSO/ LID_L1-Standard-V4-10. The ICESat-2 data are publicly available through the National Snow and Ice Data Center (NSIDC). The geolocated photon data (ATL03) are found online (https://nsidc.org/data/atl03). Datasets for this research are available in these in-text data citation references: Neumann et al. (2020). The MODIS data product can be freely downloadded from NASA Ocean Color Data Web (http://oceandata.sci.gsfc.nasa.gov accessed on 03/23/2021). The Argo floats data are freely available at http://www.coriolis.eu.org/Data-Products/Data-Delivery/Data-selection. The AMSR-E wind speeds are available through NSIDC, and MERRA-2 wind speeds can be obtained from Global Modeling and Assimilation office at https://gmao.gsfc.nasa.gov/reanalysis/MERRA-2/, accessed on 03/23/2021.

Funding for the lead author was provided by the NASA awards [grant numbers 80NSSC20K0129 and 80NSSC21K0910] for CALIPSO and ICESat-2 projects.

Competing interests: Authors declare no competing interests.

References

Abshire, J. B., Sun, X., Riris, H., Sirota, J. M., McGarry, J. F., Palm, S., et al. (2005). Geoscience Laser Altimeter System (GLAS) on the ICESat Mission: On-orbit measurement performance. *Geophysical Research Letters*, *32*(21). https://doi.org/10.1029/2005GL024028

Argo. (2020). Argo float data and metadata from Global Data Assembly Centre (Argo GDAC). *SEANOE*. https://doi.org/10.17882/42182

Behrenfeld, M. J., Hu, Y., Hostetler, C. A., Dall'Olmo, G., Rodier, S. D., Hair, J. W., & Trepte, C. R. (2013). Space-based lidar measurements of global ocean carbon stocks. *Geophysical Research Letters*, *40*(16), 4355–4360. https://doi.org/10.1002/grl.50816

Behrenfeld, M. J., Hu, Y., O/'Malley, R. T., Boss, E. S., Hostetler, C. A., Siegel, D. A., et al. (2016). Annual boom-bust cycles of polar phytoplankton biomass revealed by space-based lidar. *Nature Geosci*, *advance online publication*. https://doi.org/10.1038/ngeo2861

Behrenfeld, M. J., Hu, Y., O/'Malley, R. T., Boss, E. S., Hostetler, C. A., Siegel, D. A., et al. (2017). Annual boom-bust cycles of polar phytoplankton biomass revealed by space-based lidar. *Nature Geosci*, *10*(2), 118–122. https://doi.org/10.1038/ngeo2861

Behrenfeld, M. J., Gaube, P., Della Penna, A., O'Malley, R. T., Burt, W. J., Hu, Y., et al. (2019). Global satellite-observed daily vertical migrations of ocean animals. *Nature*, *576*(7786), 257–261. https://doi.org/10.1038/s41586-019-1796-9

Bisson, K. M., Boss, E., Westberry, T. K., & Behrenfeld, M. J. (2019). Evaluating satellite estimates of particulate backscatter in the global open ocean using autonomous profiling floats. *Optics Express*, *27*(21), 30191–30203. https://doi.org/10.1364/OE.27.030191

Bisson, K. M., Boss, E., Werdell, P. J., Ibrahim, A., & Behrenfeld, M. J. (2021). Particulate Backscattering in the Global Ocean: A Comparison of Independent Assessments. *Geophysical Research Letters*, *48*(2), e2020GL090909. https://doi.org/10.1029/2020GL090909

Chris A. Hostetler, Liu, Z., Reagan, J., Vaughan, M., Winker, D., Osborn, M., et al. (2006). CALIOP Algorithm Theoretical Basis Document Calibration and Level 1 data Products. *PC-SCI-201 Release 1.0*. https://www-calipso.larc.nasa.gov/resources/pdfs/PC-SCI-201v1.0.pdf

Claustre, H., Bishop, J., Boss, E., Stewart, B., Berthon, J.-F., Coatanoan, C., et al. (2010). *Bio-optical profiling floats as new observational tools for biogeochemical and ecosystem studies*.

Dionisi, D., Brando, V. E., Volpe, G., Colella, S., & Santoleri, R. (2020). Seasonal distributions of ocean particulate optical properties from spaceborne lidar measurements in Mediterranean and Black sea. *Remote Sensing of Environment*, *247*, 111889. https://doi.org/10.1016/j.rse.2020.111889

Getzewich, B. J., Vaughan, M. A., Hunt, W. H., Avery, M. A., Powell, K. A., Tackett, J. L., et al. (2018). CALIPSO lidar calibration at 532 nm: version 4 daytime algorithm. *Atmos. Meas. Tech.*, *11*(11), 6309–6326. https://doi.org/10.5194/amt-11-6309-2018

Hostetler, C. A., Behrenfeld, M. J., Hu, Y., Hair, J. W., & Schulien, J. A. (2018). Spaceborne Lidar in the Study of Marine Systems. *Annual Review of Marine Science*, *10*(1), 121–147. https://doi.org/10.1146/annurev-marine-121916-063335

Hovis, W. A., Clark, D. K., Anderson, F., Austin, R. W., Wilson, W. H., Baker, E. T., et al. (1980). Nimbus-7 Coastal Zone Color Scanner: System Description and Initial Imagery. *Science*, *210*(4465), 60. https://doi.org/10.1126/science.210.4465.60

Hu, C., Feng, L., & Lee, Z. (2013). Uncertainties of SeaWiFS and MODIS remote sensing reflectance: Implications from clear water measurements. *Remote Sensing of Environment*, *133*, 168–182. https://doi.org/10.1016/j.rse.2013.02.012

Hu, Y., Stamnes, K., Vaughan, M., Pelon, J., Weimer, C., Wu, D., et al. (2008). Sea surface wind speed estimation from space-based lidar measurements. *Atmos. Chem. Phys.*, *8*(13), 3593–3601. https://doi.org/10.5194/acp-8-3593-2008

Hu, Yongxiang, Powell, K., Vaughan, M., Tepte, C., Weimer, C., Beherenfeld, M., et al. (2007). Elevation information in tail (EIT) technique for lidar altimetry. *Opt. Express*, *15*(22), 14504–14515. https://doi.org/10.1364/OE.15.014504

Hunt, W. H., Winker, D. M., Vaughan, M. A., Powell, K. A., Lucker, P. L., & Weimer, C. (2009). CALIPSO Lidar Description and Performance Assessment. *Journal of Atmospheric and Oceanic Technology*, *26*(7), 1214–1228. https://doi.org/10.1175/2009JTECHA1223.1

Jamet, C., Ibrahim, A., Ahmad, Z., Angelini, F., Babin, M., Behrenfeld, M. J., et al. (2019). Going Beyond Standard Ocean Color Observations: Lidar and Polarimetry. *Frontiers in Marine Science*, *6*, 251. https://doi.org/10.3389/fmars.2019.00251

Jasinski, M. F., Stoll, J. D., Cook, W. B., Ondrusek, M., Stengel, E., & Brunt, K. (2016). Inland and Near-Shore Water Profiles Derived from the High-Altitude Multiple Altimeter Beam Experimental Lidar (MABEL). *Journal of Coastal Research*, *76*(SI), 44–55.

Kar, J., Vaughan, M. A., Lee, K.-P., Tackett, J. L., Avery, M. A., Garnier, A., et al. (2018). CALIPSO lidar calibration at 532 nm: version 4 nighttime algorithm. *Atmos. Meas. Tech.*, *11*(3), 1459–1479. https://doi.org/10.5194/amt-11-1459-2018

Lacour, L., Larouche, R., & Babin, M. (2020). In situ evaluation of spaceborne CALIOP lidar measurements of the upper-ocean particle backscattering coefficient. *Optics Express*, *28*(18), 26989–26999. https://doi.org/10.1364/OE.397126

Lu, X., Hu, Y., Trepte, C., Zeng, S., & Churnside, J. H. (2014). Ocean subsurface studies with the CALIPSO spaceborne lidar. *Journal of Geophysical Research: Oceans*, *119*(7), 4305–4317. https://doi.org/10.1002/2014jc009970

Lu, X., Hu, Y., Pelon, J., Trepte, C., Liu, K., Rodier, S., et al. (2016). Retrieval of ocean subsurface particulate backscattering coefficient from space-borne CALIOP lidar measurements. *Optics Express*, *24*(25), 29001–29008. https://doi.org/10.1364/OE.24.029001

Lu, X., Hu, Y., Yang, Y., Vaughan, M., Liu, Z., Rodier, S., et al. (2018). Laser pulse bidirectional reflectance from CALIPSO mission. *Atmospheric Measurement Techniques*, *11*(6), 3281–3296. https://doi.org/10.5194/amt-11-3281-2018

Lu, X., Hu, Y., & Yang, Y. (2019). Ocean Subsurface Study from ICESat-2 Mission. In *2019 Photonics & Electromagnetics Research Symposium - Fall (PIERS - Fall)* (pp. 910–918). https://doi.org/10.1109/PIERS-Fall48861.2019.9021802

Lu, X., Hu, Y., Yang, Y., Bontempi, P., Omar, A., & Baize, R. (2020). Antarctic spring ice-edge blooms observed from space by ICESat-2. *Remote Sensing of Environment*, 111827. https://doi.org/10.1016/j.rse.2020.111827

Lu, X., Hu, Y., Vaughan, M., Rodier, S., Trepte, C., Lucker, P., & Omar, A. (2020). New attenuated backscatter profile by removing the CALIOP receiver's transient response. *Journal of Quantitative Spectroscopy and Radiative Transfer*, 107244. https://doi.org/10.1016/j.jqsrt.2020.107244

Magruder, L., & Brunt, K. (2018). Performance Analysis of Airborne Photon- Counting Lidar Data in Preparation for the ICESat-2 Mission. *IEEE Transactions on Geoscience and Remote Sensing*, *56*(5), 2911–2918. https://doi.org/10.1109/TGRS.2017.2786659

Magruder, L., Brunt, K., & Alonzo, M. (2020). Early ICESat-2 on-orbit Geolocation Validation Using Ground-Based Corner Cube Retro-Reflectors. *Remote Sensing*, *12*, 3653. https://doi.org/10.3390/rs12213653

Markus, T., Neumann, T., Martino, A., Abdalati, W., Brunt, K., Csatho, B., et al. (2017). The Ice, Cloud, and land Elevation Satellite-2 (ICESat-2): Science requirements, concept, and implementation. *Remote Sensing of Environment*, *190*, 260–273. https://doi.org/10.1016/j.rse.2016.12.029

Morison, J., Hancock, D., Dickinson, S., Robbins, J., Roberts, L., Kwok, R., et al. (2019). ATLAS/ICESat-2 L3A Ocean Surface Height, Version 1. *Boulder, Colorado USA. NASA National Snow and Ice Data Center Distributed Active Archive Center*. https://doi.org/10.5067/ATLAS/ATL12.001

NASA, O. E. L., Ocean Biology Processing Group. NASA Goddard Space Flight. (2018). Moderate-resolution Imaging Spectroradiometer (MODIS) Aqua Downwelling Diffuse Attenuation Coefficient Data. https://doi.org/data/10.5067/AQUA/MODIS/L3M/KD/2018, Accessed on 03/17/2021

Neumann, T. A., Martino, A. J., Markus, T., Bae, S., Bock, M. R., Brenner, A. C., et al. (2019). The Ice, Cloud, and Land Elevation Satellite – 2 mission: A global geolocated photon

product derived from the Advanced Topographic Laser Altimeter System. *Remote Sensing of Environment*, *233*, 111325. https://doi.org/10.1016/j.rse.2019.111325

Neumann, T. A., Brenner, A., Hancock, D., Robbins, J., Saba, J., Harbeck, K., et al. (2020). ATLAS/ICESat-2 L2A Global Geolocated Photon Data, Version 3. https://doi.org/10.5067/ATLAS/ATL03.003 Accessed 03/23/2021

Organelli, E., Barbieux, M., Claustre, H., Schmechtig, C., Poteau, A., Bricaud, A., et al. (2017). Two databases derived from BGC-Argo float measurements for marine biogeochemical and bio-optical applications. *Earth System Science Data*, *9*(2), 861–880. https://doi.org/10.5194/essd-9-861-2017

Palm, S., Yang, Y., Herzfeld, U., Hancock, D., Hayes, A., Selmer, P., et al. (2020). ICESat-2 Atmospheric Channel Description, Data Processing and First Results. https://doi.org/10.1002/essoar.10504390.1

Pitts, M. C., Poole, L. R., & Gonzalez, R. (2018). Polar stratospheric cloud climatology based on CALIPSO spaceborne lidar measurements from 2006 to 2017. *Atmospheric Chemistry and Physics*, *18*(15), 10881–10913. https://doi.org/10.5194/acp-18-10881-2018

Popescu, S. C., Zhou, T., Nelson, R., Neuenschwander, A., Sheridan, R., Narine, L., & Walsh, K. M. (2018). Photon counting LiDAR: An adaptive ground and canopy height retrieval algorithm for ICESat-2 data. *Remote Sensing of Environment*, *208*, 154–170. https://doi.org/10.1016/j.rse.2018.02.019

Righetti, D., Vogt, M., Gruber, N., Psomas, A., & Zimmermann, N. E. (2019). Global pattern of phytoplankton diversity driven by temperature and environmental variability. *Science Advances*, *5*(5), eaau6253. https://doi.org/10.1126/sciadv.aau6253

Sullivan, C. W., Arrigo, K. R., McClain, C. R., Comiso, J. C., & Firestone, J. (1993). Distributions of Phytoplankton Blooms in the Southern Ocean. *Science*, *262*(5141), 1832. https://doi.org/10.1126/science.262.5141.1832

Vallina, S. M., Follows, M. J., Dutkiewicz, S., Montoya, J. M., Cermeno, P., & Loreau, M. (2014). Global relationship between phytoplankton diversity and productivity in the ocean. *Nature Communications*, *5*(1), 4299. https://doi.org/10.1038/ncomms5299

Werdell, P. J., Franz, B. A., Lefler, J. T., Robinson, W. D., & Boss, E. (2013). Retrieving marine inherent optical properties from satellites using temperature and salinity-dependent backscattering by seawater. *Opt. Express*, *21*(26), 32611–32622. https://doi.org/10.1364/OE.21.032611

Winker, D. M., Pelon, J., Coakley, J. A., Ackerman, S. A., Charlson, R. J., Colarco, P. R., et al. (2010). The CALIPSO Mission: A Global 3D View of Aerosols and Clouds. *Bulletin of the American Meteorological Society*, *91*(9), 1211–1229. https://doi.org/10.1175/2010bams3009.1

Winker, David M., Vaughan, M. A., Omar, A., Hu, Y., Powell, K. A., Liu, Z., et al. (2009). Overview of the CALIPSO Mission and CALIOP Data Processing Algorithms. *Journal of Atmospheric and Oceanic Technology*, *26*(11), 2310–2323. https://doi.org/10.1175/2009jtecha1281.1